A high-resolution analysis of the $\tilde{A}\,^2A'$–$\tilde{X}\,^2A'$ transition of CaSH by laser excitation spectroscopy

C. N. Jarman and P. F. Bernath[a),b)]
Department of Chemistry, University of Arizona, Tucson, Arizona 85712

(Received 3 November 1992; accepted 20 January 1993)

The high resolution spectrum of the $\tilde{A}\,^2A'$–$\tilde{X}\,^2A'$ transition of CaSH has been recorded near 650 nm using laser excitation spectroscopy with selected fluorescence detection. While both *a*-type and *b*-type rotational transitions have been observed, extensive measurements have been made for the *b*-type transitions up to $K_a' = 4$ and $K_a'' = 5$. Altogether over 3000 rotational lines have been measured and fitted with an *A*-reduced Hamiltonian. The $\tilde{X}\,^2A'$ state has rotational constants $A=9.693\,322(46)$ cm^{-1}, $B=0.141\,864\,7(33)$ cm^{-1}, and $C=0.139\,581\,0(33)$ cm^{-1}. The $\tilde{A}\,^2A'$ state has a band origin at $15\,380.284\,7(2)$ cm^{-1}, and effective values for the rotational constants $A=9.090\,808(78)$ cm^{-1}, $B=0.147\,459\,8(34)$ cm^{-1}, and $C=0.144\,804\,2(34)$ cm^{-1}. An approximate r_0 structure for CaSH is discussed. The $\tilde{A}\,^2A'$ state is the lower energy Renner–Teller component of the "$\tilde{A}\,^2\Pi$" state of the hypothetical linear CaSH molecule, and consequently was found to have a relatively large positive value for the spin–rotation parameter ϵ_{aa} at $3.445\,69(26)$ cm^{-1}. The upper asymmetry component of the F_1 spin component of the $K_a=1$ stack and the F_2 spin component of the $K_a=0$ stack in the $\tilde{A}\,^2A'$ state perturb each other with an avoided crossing between $J=37.5$ and $J=38.5$. These two spin components interact through the off-diagonal $|\epsilon_{ab}+\epsilon_{ba}|/2$ element of the spin–rotation tensor. For CaSH, the $\tilde{A}\,^2A'$ state has $|\epsilon_{ab}+\epsilon_{ba}|/2=0.065\,915(46)$ cm^{-1}.

INTRODUCTION

In contrast to the extensive amount of research work devoted to the high resolution spectroscopic study of gas phase alkaline earth monohydroxides[1–9] in recent years, there has been only one low resolution spectroscopic investigation of the isovalent monohydrosulfides.[10] The parent dihydrosulfides are important in industrial processes—an aqueous solution of $Ca(SH)_2$ has been used both in the removal of SO_2 and SO_3 from H_2SO_4 (Ref. 11) and also in the recovery of sulfur from underground ore deposits.[12] The nature of the metal–sulfur bond is also important to the inorganic chemist and in the study of biological systems such as the active sites of proteins. It is clear, therefore, that a more detailed probe of the structures and properties of metal containing sulfur compounds is desirable.

In the only previous spectroscopic study of CaSH by Fernando *et al.*,[10] approximate term energies and Ca–S stretching frequencies were determined from low resolution spectra for the ground and the three lowest excited electronic states. The values they obtained were in good agreement with the *ab initio* electron propagator calculations of Ortiz.[13] However, the low resolution spectra did not provide any means to unequivocally determine the symmetry or geometry of the electronic states. Some of this information came from a preliminary investigation of the $\tilde{B}\,^2A''$–$\tilde{X}\,^2A'$ transition at high resolution by Ram and Bernath.[14] In the work reported here, we have concentrated on recording and analyzing the lowest-lying $\tilde{A}\,^2A'$–$\tilde{X}\,^2A'$ transition.

According to Ortiz's *ab initio* calculations,[13] the $\tilde{A}\,^2A'$ and $\tilde{B}\,^2A''$ states of CaSH are well described by a one electron picture in which the unpaired electron is localized near the Ca atom in a calcium centered orbital of approximate p_π symmetry. This orbital is slightly hybridized away from the SH ligand by mixing with calcium d_π functions. The $\tilde{A}\,^2A'$ state corresponds to the component of the p_π orbital in the plane of the molecule, and the $\tilde{B}\,^2A''$ state corresponds to the out-of-plane component. Since CaSH is bent, the in-plane p_π and the out-of-plane p_π orbitals have different energies. Molecular rotation about the *a* axis will cause these two states to mix and hence induce some K_a dependent orbital angular momentum into both of these states. The magnitude of this orbital momentum will be determined by the energy separation between the $\tilde{A}\,^2A'$ and $\tilde{B}\,^2A''$ states. A similar effect has been discussed by Whitham and Jungen[15] in their study of the corresponding states of $CaNH_2$.

EXPERIMENT

CaSH was produced in a conventional Broida oven[16] by the reaction of excited Ca atoms with H_2S. Two lasers were used in this study, one to promote the chemical reaction by exciting a Ca atomic transition, and another to probe the molecular transitions. The first laser was a Coherent 699-01 dye laser pumped by 6 W of all lines visible radiation from a Coherent Innova 70 argon ion laser and

[a)]Camille and Henry Dreyfus Teacher–Scholar.
[b)]Also Department of Chemistry, University of Waterloo, Waterloo, Ontario, Canada N2L 3G1.

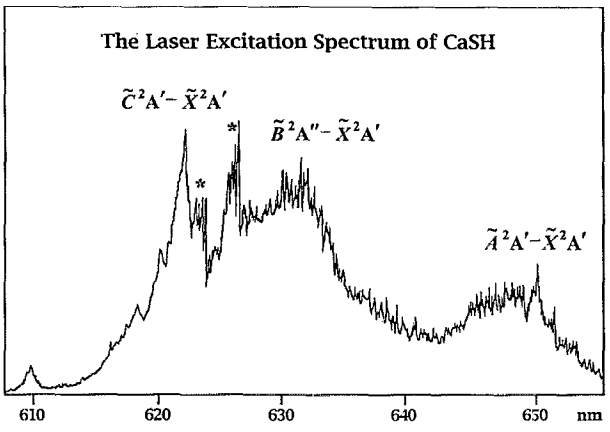

FIG. 1. The low resolution laser excitation spectrum of CaSH. The features marked with asterisks are the two spin components of the $\tilde{A}\,^2\Pi$–$\tilde{X}\,^2\Sigma^+$ transition of CaOH, produced as an impurity. The feature at 610 nm is due to transitions to one quantum in the Ca–S stretch of the $\tilde{C}\,^2A'$ state.

operating in linear mode with DCM dye. The bandwidth of this laser was narrowed (triple mode operation) with an étalon, and the laser was tuned to the $^3P_1$–$^1S_0$ atomic transition of Ca at 657.3 nm. The laser beam was directed into the alumina crucible containing the Ca metal in the Broida oven. When H_2S was added at the top of the crucible, a white chemiluminescent flame appeared characteristic of CaSH production.

The probe laser was a Coherent 699-29 ring dye laser operating with DCM dye and pumped by 7 W of 488 nm radiation from a Coherent Innova 200 argon ion laser. The laser beam was focused vertically into the CaSH flame, and the laser induced fluorescence was focused onto the entrance slits of a 0.64 m monochromator. Care was taken to separate the atomic pump laser beam from the molecular probe laser beam so that the entrance slits of the monochromator could act as a spatial filter and remove most of the Ca atomic fluorescence. The molecular laser induced fluorescence was then dispersed by the monochromator, detected with a photomultiplier tube, and processed by photon counting electronics.

Initially, we scanned the probe laser broad band (1 cm^{-1} resolution) and detected the laser induced fluorescence through the monochromator in zeroth order, effectively recording the total molecular fluorescence. The spectrum is depicted in Fig. 1, from which it is clear that the two lowest-lying electronic transitions $\tilde{A}\,^2A'$–$\tilde{X}\,^2A'$ and $\tilde{B}\,^2A''$–$\tilde{X}\,^2A'$ cover a wider spectral range than the third electronic transition $\tilde{C}\,^2A'$–$\tilde{X}\,^2A'$. We attribute this observation to larger amounts of perpendicular rotational structure in $\tilde{A}\,^2A'$–$\tilde{X}\,^2A'$ and $\tilde{B}\,^2A''$–$\tilde{X}\,^2A'$, compared to the parallel $\tilde{C}\,^2A'$–$\tilde{X}\,^2A'$ transition. This fact will make the $\tilde{C}\,^2A'$–$\tilde{X}\,^2A'$ transition very difficult to analyze because many a-type rotational transitions will lie in a small wavelength range. The spectrum also displays fluorescence from the $\tilde{A}\,^2\Pi$–$\tilde{X}\,^2\Sigma$ system of CaOH, produced as an impurity.

We then scanned the probe laser at high resolution, and recorded selected pieces of the spectrum near 650 nm as a function of wave number using Coherent's PC-Autoscan software. These scans had a high signal-to-noise ratio, but the incredible density of molecular lines made them difficult to interpret. However, certain features in these spectra were stronger than others and looked as if they might be bandheads. Our next step was to record dispersed fluorescence spectra by fixing the probe laser on each of these bandhead features in turn, and scanning the monochromator for each laser position. The majority of the dispersed fluorescence in these spectra was resonant and all the scans contained a resonant feature near 650 nm, one resonant feature to higher wavelength, and one to lower wavelength. We concluded that we were seeing an *ab* hybrid rovibronic transition between two bent electronic states with similar A rotational constants—the laser was probing different upper K_a stacks, and the fluorescence was obeying $\Delta K_a = \pm 1,0$ selection rules.

High resolution (1 MHz laser bandwidth) spectra were then recorded by fixing the monochromator on one of the resonant features found in a dispersed fluorescence spectrum and scanning the laser for 20 cm^{-1} around its original position. In this way, we could selectively record fluorescence from different upper K_a stacks. The Doppler-limited spectra were stored as a function of wave number using Coherent's PC-Autoscan software. The wave number scale was calibrated by simultaneously recording the iodine absorption spectrum and comparing the measured line positions to the published line list[17] correcting for the -0.0056 cm^{-1} shift.[18] The high resolution data files were converted to ASCII format for use with the data reduction package PC-DECOMP developed at the National Solar Observatory by Brault. Each rovibronic line in the spectra was first fit to a Voigt profile using PC-DECOMP, and then the line positions and intensities were used as input to PC-LOOMIS, an interactive color Loomis–Wood[19] program written by one of the authors (Jarman) to pick out rotational branches.

ANALYSIS OF THE SPECTRA

At first we recorded and analyzed only the b-type $K_a \geqslant 2$ transitions in which there was expected to be negligible asymmetry doubling. These spectra did indeed prove to be both the easiest to record and the easiest to analyze. The spectra were recorded by scanning the laser over the transitions with $K_a'' = K_a' - 1$, while keeping the monochromator on the resonant bandheads with $K_a'' = K_a' + 1$ (see Fig. 2). After recording these spectra, the positions of the laser and monochromator were switched to record $\Delta K_a = -1$ spectra. Because the laser and the monochromator positions are spaced by approximately $4A''K_a'$, (e.g., ~ 80 cm^{-1} for $K_a' = 2$), we could open the monochromator slits without fear of seeing the laser. Thus the entire J structure of the bandhead could lie in the monochromator bandpass, and so the entire J structure for the connecting K_a' subband could be recorded in one scan.

The initial analysis of these spectra was simplified by the large value for the effective A rotational constant in both states. This allowed each $K_a \neq 0$ stack to be treated, in

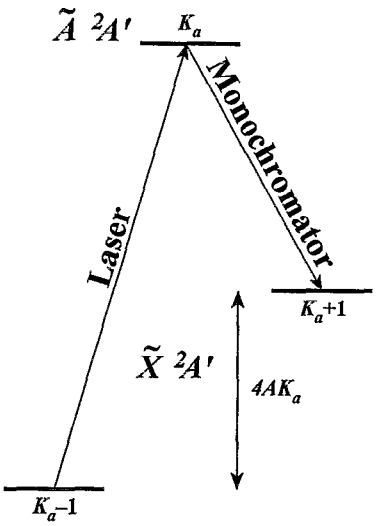

FIG. 2. A schematic showing the positions of the laser and monochromator in recording high resolution $\Delta K_a=+1$ spectra.

first approximation, as an independent $^2\Pi$ state with a spin–orbit splitting of $\epsilon_{aa}K_a$. It quickly became apparent by comparing different spectra that the value for ϵ_{aa} in the ground state was zero, just as expected for an isolated state that correlates to a $^2\Sigma^+$ state in the linear configuration. By analogy with the ground states of CaOH, and CaF, the value for the spin–rotation constant $(\epsilon_{bb}+\epsilon_{cc})/2=\gamma$ ($\gamma''=0.0012$ cm^{-1} for CaOH and $\gamma''=0.0013$ cm^{-1} for CaF) was also expected to be small, and so the F_1 and F_2 components were expected to be almost coincident in energy. Thus the $K_a\neq 0$ stacks for the ground state were expected to behave like Hund's case (b) $^2\Pi$ states. However, the value of ϵ_{aa} in the upper state was found to be relatively large, and so the $K_a\neq 0$ stacks for the upper state were more like Hund's case (a) $^2\Pi$ states. This is evident in Figs. 3 and 4, which show the two different spin components of the 4–3 subband. The energy separation between the P_1+Q_{12} and the Q_2+P_{21} bandheads is about 13 cm^{-1},

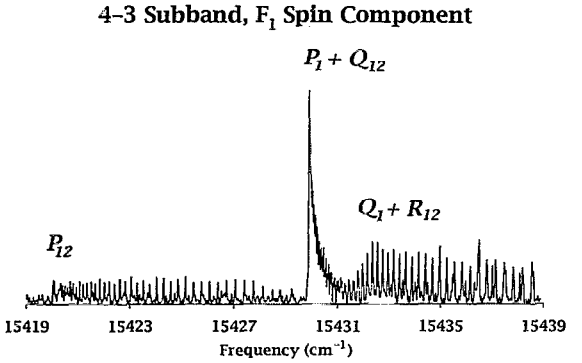

FIG. 3. The high resolution spectrum of the F_1 component of the 4–3 subband of the $\tilde{A}\,^2A'$–$\tilde{X}\,^2A'$ transition in CaSH. The spectrum was taken by fixing the monochromator on the P_1 bandhead of the 4–5 subband.

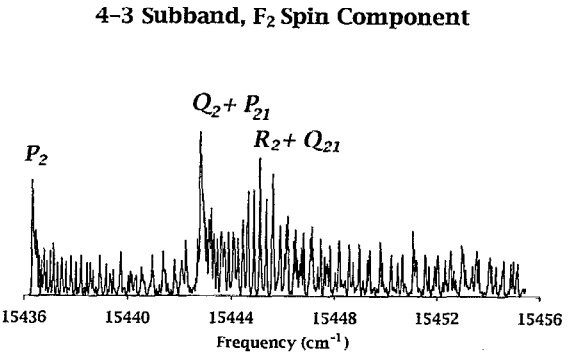

FIG. 4. The high resolution spectrum of the F_2 component of the 4–3 subband of the $\tilde{A}\,^2A'$–$\tilde{X}\,^2A'$ transition in CaSH. The spectrum was taken by fixing the monochromator on the Q_2 bandhead of the 4–5 subband.

and this gives an approximate value for ϵ'_{aa} of ~ 3.25 cm^{-1}. The branches are labeled using the customary $^2\Pi$–$^2\Pi$ branch notation.[20]

Thus the 4–3, 4–5, 3–4, 3–2, and 2–3 subbands were initially analyzed as separate $^2\Pi(a)$–$^2\Pi(b)$ electronic transitions of a diatomic molecule, with strong Q_2, Q_1, R_2, R_1, P_2, and P_1 branches, and weak Q_{21}, Q_{12}, R_{21}, P_{21}, R_{12}, and P_{12} satellite branches. Most of these satellite branches, except R_{21} and P_{12}, lay beneath stronger regular branches, and so the spectra displayed four distinct rotational branches in two separate regions split by the effective spin–orbit constant—P_2, (Q_2 and P_{21}), (R_2 and Q_{21}), and R_{21} in one region, and P_{12}, (P_1 and Q_{12}), (Q_1, and R_{12}), and R_1 in the other. The satellite branches also became weaker as K'_a went from 4 to 2, in keeping with the increasing Hund's case (b) character (smaller effective spin–orbit splitting) of the lower K'_a stacks.

Using this model, it was possible to assign J quantum numbers to every rovibronic transition in the subbands, and to determine values for the effective spin–orbit constants in the upper K_a stacks. Because these values agreed very well with the $\epsilon_{aa}K_a$ formula, we next proceeded to fit these subbands together using a doublet asymmetric rotor Hamiltonian. The A-reduced rotational Hamiltonian of Watson[21] was used together with Brown and Sears'[22] A-reduced form for the spin–rotation part of the Hamiltonian

$$\tilde{H}^{(2)}_{\rm sr}=\epsilon_{aa}N_aS_a+\epsilon_{bb}N_bS_b+\epsilon_{cc}N_cS_c+1/2(\epsilon_{ab}+\epsilon_{ba})\times(N_bS_a+N_aS_b),$$

$$\tilde{H}^{(4)}_{\rm sr}=\Delta^s_N\mathbf{N}^2(\mathbf{N}\cdot\mathbf{S})+1/2\Delta^s_{NK}(\mathbf{N}^2N_zS_z+N_zS_z\mathbf{N}^2)+\Delta^s_{KN}N_z^2(\mathbf{N}\cdot\mathbf{S})+\Delta^s_KN_z^3S_z+\delta^s_N(N_+^2+N_-^2)\times(\mathbf{N}\cdot\mathbf{S})+1/2\delta^s_K[(N_+^2+N_-^2)N_zS_z+N_zS_z(N_+^2+N_-^2)].$$

A computer program was written that set up the Hamiltonian matrix in a total parity conserving basis set, using the matrix elements listed in Hirota's book on free radicals.[23] In this fit, we deliberately excluded the high J tran-

sitions of the 3–2 and 2–3 subbands, and constrained the off-diagonal matrix elements in K_a to zero in both electronic states. The transitions fit very well and this augured well for the continuation of the analysis to lower K_a.

The next step was to record and analyze the 2–1 subband. This was easy, because we already knew the location of the connecting 2–3 bandheads. The assignment was relatively straightforward, and when we included this subband in our global fit, we determined values for the asymmetry in the rotational constants $(B-C)/2$ in the ground state. We then predicted the line positions for the 0–1 and the 0–0 subbands, but this prediction was not very accurate because it involved extrapolation from $K_a' = 2$ in the upper state. However, it did provide a good starting point to locate the bandheads, which in turn allowed us to scan the laser through the 0–0 and the 0–1 subbands with the monochromator on the bandheads in the connecting subband.

The rotational structure for $K_a=0$ in both the ground and excited states is very similar to that seen in a $^2\Sigma^+$ state of a diatomic molecule, and hence the 0–0 subband looked like a $^2\Sigma^+$–$^2\Sigma^+$ transition with R_2, R_1, P_2, and P_1 branches. The 0–1 subband looked like a $^2\Sigma^+$–$^2\Pi(b)$ transition with additional Q_2, Q_1, and satellite branches. Both of these subbands revealed that the F_2 component of the $K_a' = 0$ stack was perturbed by a higher energy spin component crossing below it between $J=37.5$ and $J=38.5$. Hence, we added to the global data set all of the F_1 transitions, but only transitions up to $J=19.5$ in the F_2 component. We also included the high J $K_a=2$ transitions that we omitted from previous fits, fixed the value for $(B-C)/2$ in the upper state to the same as that for the ground state, and refit the data.

We then predicted and recorded the spectra for the 1–0, 1–1, and 1–2 subbands, using the same techniques that we used previously. However, because the spacing between the upper state spin components was only about 3.5 cm^{-1}, it was impossible to record each component separately, and so the spectra were complicated by many overlapping rotational branches. The predictions were not very helpful in sorting out the mess because the energies of the $K_a' = 1$ spin components depend on the first order corrections of the off-diagonal $\Delta K_a = \pm 2$ matrix elements. We had made a reasonable guess for the value of $(B-C)/2$, but had no idea of the value or even the sign for the $(\epsilon_{bb}-\epsilon_{cc})/2$ parameter associated with the $\Delta K_a = \pm 2$ matrix elements. The J assignment was made by finding rotational branches in PC-LOOMIS, and then matching differences between these branches to ground state combination differences.

The Loomis–Wood plots revealed that the upper asymmetry component of the F_1 spin component of the $K_a' = 1$ stack was perturbed by a lower energy spin component crossing above it between $J=37.5$ and $J=38.5$. This is the exact opposite effect to what we observed in the F_2 component of the $K_a' = 0$ stack, and confirmed that the perturbations were internal to the upper electronic state, a direct result of the off-diagonal $|\epsilon_{ab}+\epsilon_{ba}|/2$ term in the Hamiltonian. This term is identically zero for molecules of orthorhombic symmetry such as $CaNH_2$, but nonzero for molecules such as CaSH with C_s symmetry. Similar perturbations have been observed in the millimeter-wave spectrum of the ground state of HCCCO.[24] We added all the perturbed and nonperturbed $K_a' = 1$ transitions together with the perturbed $K_a' = 0$ transitions to the global data set, and refit the data to obtain the spectroscopic constants listed in Table I. The fit to the individual transitions is available from PAPS,[25] or from the authors upon request. The term values for all the spin components of $K_a=0$ and $K_a=1$ relative to those of the F_1 $K_a=0$ spin component are plotted against $J+1/2$ in Fig. 5(a) for the $\tilde{X}\,^2A'$ state, and in Fig. 5(b) for the $\tilde{A}\,^2A'$ state. The upper state plot clearly shows the interaction of the upper asymmetry F_1 component of the $K_a' = 1$ stack with the F_2 component of the $K_a' = 0$ stack. The energy of the lowest J levels for the F_1 and F_2 spin components in each K_a stack is plotted for the $\tilde{A}\,^2A'$ electronic state in Fig. 6. The quadratic dependence of the energy and the linear dependence of the F_2–F_1 splitting on K_a is clearly seen in this figure.

TABLE I. The effective spectroscopic constants of the $\tilde{X}\,^2A'$ states of CaSH.

	$\tilde{X}\,^2A'$	$\tilde{A}\,^2A'$
T	0.0	15 380.284 67(23)
A	9.693 322(46)	9.090 808(78)
$(B+C)/2$	0.140 722 8(33)	0.146 132 0(33)
$(B-C)/2$	0.001 141 86(37)	0.001 327 8(10)
$D_K\times10^{-4}$	8.843(16)	4.629(36)
$D_{NK}\times10^{-5}$	1.172 5(18)	1.993 8(28)
$D_N\times10^{-7}$	0.953(10)	1.265(10)
ϵ_{aa}		3.445 69(26)
$(\epsilon_{bb}+\epsilon_{cc})/2$	0.001 388 6(69)	0.051 676(17)
$(\epsilon_{bb}-\epsilon_{cc})/2$	0.000 205(26)	−0.026 569(29)
$\lvert\epsilon_{ab}+\epsilon_{ba}\rvert/2$		0.065 915(46)
$D_K^S\times10^{-3}$		−2.077(77)
$D_{KN}^S\times10^{-4}$		−5.61(76)
$D_{NK}^S\times10^{-5}$		2.96(58)
σ	0.0040	

DISCUSSION

The $\tilde{A}\,^2A'$ and the $\tilde{B}\,^2A''$ electronic states of CaSH correlate with the $\tilde{A}\,^2\Pi$ state and the $\tilde{C}\,^2A'$ state correlates with the $\tilde{B}\,^2\Sigma^+$ state of the hypothetical linear molecule. All three of these states arise mainly from an atomic ^2P state of Ca^+, and, in the "pure precession" limit, the $\tilde{C}\,^2A'$ state arises from a single electron in the $4p_\sigma$ orbital of Ca^+ aligned along the Ca–S bond, and the $\tilde{A}\,^2A'$ and the $\tilde{B}\,^2A''$ states arise from a single electron in the $4p_\pi$ orbitals of Ca^+, aligned in and out of the molecular plane, respectively. In the rotating molecule, these electronic states interact by a mechanism analagous to Coriolis coupling between vibrational levels in a single electronic state. Rotation about the a axis of the molecule couples the $\tilde{A}\,^2A'$ and the $\tilde{B}\,^2A''$ states, and induces a net orbital angular momentum into each state. This orbital angular momentum then couples with the spin of the electron to yield an effective spin–orbit parameter that depends linearly on the amount of a-axis rotation K_a. Whitham and Jungen, in their work on the $\tilde{A}\,^2B_2$–$\tilde{X}\,^2A_1$ and $\tilde{B}\,^2B_1$–$\tilde{X}\,^2A_1$ electronic

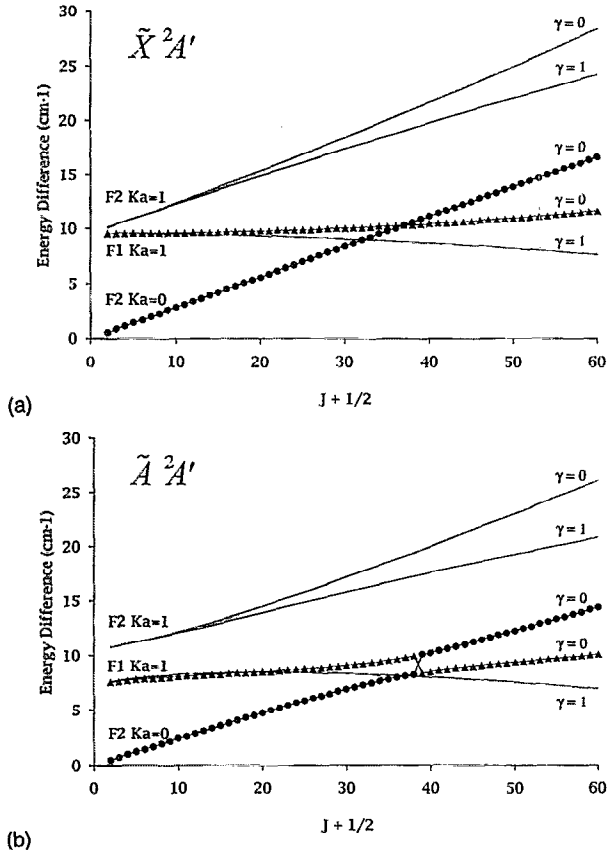

FIG. 5. Plots for the (a) $\tilde{X}\,^2A'$ and (b) $\tilde{A}\,^2A'$ states of the calculated term energies of the K_a=0,1 stacks relative to the energy of the F_1 spin component of K_a=0. The asymmetry components are labeled by $\gamma=K_a+K_c-N$. The γ=0 asymmetry components of the F_2, K_a=0 and the F_1, K_a=1 spin components cross in both electronic states. Because both of these asymmetry components have the same total parity $(-1)^{K_c}$ for a given J, they interact in an avoided crossing. The effect is too small to be seen in the $\tilde{X}\,^2A'$ state, but is obvious in the $\tilde{A}\,^2A'$ state. The rotational lines of the interacting components are marked with dots and triangles to highlight the crossing.

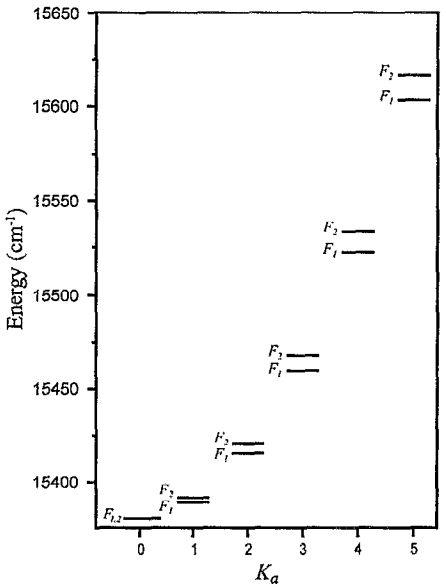

FIG. 6. A plot of the term values of the lowest rotational lines in each K_a stack of the $\tilde{A}\,^2A'$ state.

transitions of $CaNH_2$,[15] have derived formulas for the effect of this interaction on the A and ϵ_{aa} spectroscopic constants derived for the $\tilde{A}$ and $\tilde{B}$ states in the pure precession limit

$$A^{\rm Spec}=A\mp\frac{4\Lambda^2A^2}{\Delta E_{\tilde{B}-\tilde{A}}},\quad \epsilon_{aa}=\pm\frac{4\Lambda^2AA^{\rm so}}{\Delta E_{\tilde{B}-\tilde{A}}}.$$

Here, A is the "true" value for the a-axis rotation constant, Λ is the component of the orbital angular momentum on the a axis, $A^{\rm so}$ is the value for the spin–orbit interaction in the parent $^2\Pi$ state, and $\Delta E_{\tilde{B}-\tilde{A}}$ is the energy difference $E(\tilde{B})-E(\tilde{A})$. In these formulas, the top sign refers to the $\tilde{A}$ state and the lower to the $\tilde{B}$ state.

Independent of the work reported here, Ram and Bernath[14] have recorded some high resolution spectra of the $\tilde{B}\,^2A''$–$\tilde{X}\,^2A'$ system, and a preliminary analysis of this data has yielded a band origin position at 15 860 cm^{-1}, and an effective spectroscopic A constant of 10.14 cm^{-1}. This gives A(true)=9.615 cm^{-1} and ΔE=480 cm^{-1} for use in the above formulas, which in turn gives Λ=0.83 and $A^{\rm so}$=63 cm^{-1}. For a pure $^2\Pi$ parent, the value for Λ should be unity and the fact that the formula gives a value less than this indicates that the "pure precession" approximation is not completely valid. However, the value for the spin–orbit constant $A^{\rm so}$=63 cm^{-1} is consistent with the measured values of 71 and 66 cm^{-1} for CaF and CaOH, respectively. It is interesting to perform the same calculations for $CaNH_2$ using Whitham and Jungen's data.[15] They found that ϵ_{aa}=8.1 cm^{-1}, A(true)=13 cm^{-1}, and ΔE=422 cm^{-1}, and the above formulas give Λ=1.0 and $A^{\rm so}$=66 cm^{-1}. The value of Λ=0.83 can be rationalized by "orbital mixing" between the $\tilde{A}\,^2A'$ and $\tilde{C}\,^2A'$ states in the nonrotating molecule. This interaction will tend to reduce Λ from 1 in the $\tilde{A}$ state and increase it from zero in the $\tilde{C}$ state. Such an interaction is not possible in $CaNH_2$, where the $\tilde{A}\,^2B_2$ and $\tilde{C}\,^2A_1$ states have different symmetries.

In a similar fashion, rotation about the b axis causes interactions between the $\tilde{C}$ and $\tilde{B}$ states, and rotation about the c axis causes interactions between the $\tilde{C}$ and $\tilde{A}$ states. In the pure precession limit, these interactions give rise to the following values for ϵ_{bb} in the $\tilde{C}$ and $\tilde{B}$ states and ϵ_{cc} in the $\tilde{C}$ and $\tilde{A}$ states:

$$\epsilon_{bb}=\pm\frac{2l(l+1)BA^{\rm so}}{\Delta E_{\tilde{C}-\tilde{B}}},\quad \epsilon_{cc}=\pm\frac{2l(l+1)CA^{\rm so}}{\Delta E_{\tilde{C}-\tilde{A}}},$$

where l is the electronic orbital angular momentum quantum number (1 for p orbitals). In these formulas, the top sign again refers to the lower of the two states (i.e., to the $\tilde{B}$ state in the ϵ_{bb} formula and to the $\tilde{A}$ state in the ϵ_{cc} formula). In the pure precession limit, ϵ_{aa}=0 in the $\tilde{C}$ state, ϵ_{bb}=0 in the $\tilde{A}$ state, and ϵ_{cc}=0 in the $\tilde{B}$ state. Using l=1, $A^{\rm so}$=63 cm^{-1}, and $E(\tilde{C})$=16 070 cm^{-1} from the observed center of the $\tilde{C}\,^2A'$–$\tilde{X}\,^2A'$ transition in the low resolution spectrum, these formulas predict that ϵ_{bb}=0 cm^{-1}, and ϵ_{cc}=0.053 cm^{-1}, in the $\tilde{A}\,^2A'$ state compared to

TABLE II. The calculated r_0 structure of CaSH in the $\tilde{X}\,^2A'$ and $\tilde{A}\,^2A'$ states compared to the theoretical values for the r_e structure in the $\tilde{X}\,^2A'$ ground state.

	$r_e\,\tilde{X}\,^2A'$[a]	$r_0\,\tilde{X}\,^2A'$	$r_0\,\tilde{A}\,^2A'$
∠Ca–S–H	100.0°	96.6°	94.6°
S–H(Å)	1.346	1.346[b]	1.346[b]
Ca–S(Å)	2.614	2.560	2.513

[a]Reference 13.
[b]Fixed to the *ab initio* value of Ref. 13.

TABLE III. The principal elements of the spin–rotation and the g tensors $\epsilon_{\alpha\alpha}$ and $g_{\alpha\alpha}$ predicted from Curl's relation.

	$\tilde{X}\,^2A'$	$\tilde{A}\,^2A'$
ϵ_{aa}	0.0	3.445 69(26)
ϵ_{bb}	0.001 594(27)	0.025 107(34)
ϵ_{cc}	0.001 184(27)	0.078 245(34)
g_{aa}	2.002 32	1.823 14
g_{bb}	1.996 70	1.917 19
g_{cc}	1.998 08	1.732 14

their respective experimental values of 0.025 107(34) and 0.078 245(34) cm^{-1}. Both experimental values are larger than the prediction by 0.025 cm^{-1}, but are in good qualitative agreement.

Having obtained the "true" value for the A constant in the $\tilde{A}\,^2A'$ state, we used it together with the spectroscopic values for B and C to produce an approximate r_0 structure for the $\tilde{A}\,^2A'$ state. We then repeated the determination for the ground state using the spectroscopically determined value of A''. In each case, we constrained the geometry to be planar by calculating the geometry first with (I_A,I_B) and then with (I_A,I_C) pairs. We were also forced to constrain the S–H bond distance to 1.346 Å (Ref. 13) in both states. Because the molecule is an asymmetric top, no simple formulas exist for generating bond lengths and bond angles from values of I_A and I_B, and so a nonlinear least squares fitting program was written which built up the moment of inertia tensor in terms of bond lengths and bond angles according to the formulas given in Gordy and Cook,[26] diagonalized it, compared eigenvalues with the input values of I_A and I_B, and used this difference vector to generate improved bond lengths and angles. The r_0 structure for both states is compared to the *ab initio* r_e structure of the $\tilde{X}\,^2A'$ state calculated by Ortiz[13] in Table II. The agreement for the ground state is satisfactory considering the approximate nature of both calculations. A better r_s structure can only be obtained by analyzing different isotopomers of CaSH, particularly CaSD. At present, we have no plans to record these spectra.

We have also used the measured values for the spin–rotation tensor elements to calculate values for the g tensor according to Curl's formula[27]

$$g_{\alpha\alpha}\approx g_e-\frac{\epsilon_{\alpha\alpha}}{2B_\alpha},$$

where $g_e=2.002\,32$ and B_α is the rotational constant in wave numbers. The predicted values are reproduced in Table III. We hope these values will provide stimulus for others to record the electron-spin resonance (ESR) spectrum of CaSH.

CONCLUSIONS

We have performed the first high resolution spectroscopic analysis of the CaSH molecule, generating spectroscopic constants for the $\tilde{A}\,^2A'$ and $\tilde{X}\,^2A'$ states. CaSH is the first metal hydrosulfide to be rotationally analyzed and is an excellent example of a doublet asymmetric top with spin–rotation constants of moderate size. The $\tilde{A}\,^2A'$ state correlates with the lower energy Renner–Teller component of the $\tilde{A}\,^2\Pi$ state of the isovalent molecules CaOH and CaF. An internal avoided crossing was seen between the upper asymmetry F_1 spin component of the $K_a=1$ stack, and the F_2 spin component of the $K_a=0$ stack. It seems that this type of internal perturbation is characteristic of doublet asymmetric top spectra.

ACKNOWLEDGMENTS

This work was supported by the National Science Foundation (CHE-8913785), the Natural Science and Engineering Research Council of Canada, and the Centres of Excellence in Molecular and Interfacial Dynamics.

[1] R. C. Hilborn, Z. Qingshi, and D. O. Harris, J. Mol. Spectrosc. **97**, 73 (1983).
[2] P. F. Bernath and S. Kinsey-Nielsen, Chem. Phys. Lett. **105**, 663 (1984).
[3] P. F. Bernath and C. R. Brazier, Astrophys. J. **288**, 373 (1985).
[4] R. A. Hailey, C. N. Jarman, W. T. M. L. Fernando, and P. F. Bernath, J. Mol. Spectrosc. **147**, 40 (1991).
[5] J. A. Coxon, M. Li, and P. I. Presunka, J. Mol. Spectrosc. **150**, 33 (1991).
[6] T. C. Steimle, D. A. Fletcher, K. Y. Jung, and C. T. Scurlock, J. Chem. Phys. **96**, 2556 (1992).
[7] J. A. Coxon, M. Li, and P. I. Presunka, Mol. Phys. **76**, 1463 (1992).
[8] L. M. Ziurys, W. L. Barclay, and M. A. Anderson, Astrophys. J. **384**, L63 (1992)
[9] C. N. Jarman and P. F. Bernath, J. Chem. Phys. **97**, 1711 (1992).
[10] W. T. M. L. Fernando, R. S. Ram, L. C. O'Brien, and P. F. Bernath, J. Phys. Chem. **95**, 2665 (1991).
[11] L. Pawlowska, R. Chamer, and S. Musial, Chem. Abs. **111**, 159536m (1989).
[12] C. W. Weston and J. W. Wen, Chem. Abs. **108**, 153016h (1988).
[13] J. V. Ortiz, Chem. Phys. Lett. **169**, 116 (1990).
[14] R. S. Ram and P. F. Bernath (unpublished results).
[15] C. J. Whitham and Ch. Jungen, J. Chem. Phys. **93**, 1001 (1990).
[16] J. B. West, R. S. Bradford, J. D. Eversole, and C. R. Jones, Rev. Sci. Instrum. **46**, 164 (1975).
[17] S. Gerstenkorn and P. Luc, *Atlas du Spectra d'Absorption de la Molecule d'Iode* (CNRS, Paris, 1978).
[18] S. Gerstenkorn and P. Luc, Rev. Phys. Appl. **14**, 791 (1979).
[19] F. W. Loomis and R. W. Wood, Phys. Rev. **32**, 223 (1928).
[20] G. Herzberg, *Molecular Spectra and Molecular Structure* (Krieger, Malabar, FL, 1989), Vol. 1.
[21] J. K. G. Watson, J. Chem. Phys. **46**, 1935 (1967).
[22] J. M. Brown and T. J. Sears, J. Mol. Spectrosc. **75**, 111 (1979).
[23] E. Hirota, *High-Resolution Spectroscopy of Transient Molecules* (Springer, Berlin, 1985).
[24] A. L. Cooksy, J. K. G. Watson, C. A. Gottlieb, and P. Thaddeus, J. Mol. Spectrosc. **153**, 610 (1992).

[25] See AIP document no. PAPS JCPSA-98-6697-21 for 21 pages of tables. Order by PAPS number and journal reference from American Institute of Physics, Physics Auxiliary Publication Service, 335 East 45th Street, New York, NY 10017. The price is $1.50 for each microfiche (60 pages) or $5.00 for photocopies of up to 30 pages, and $0.15 for each additional page over 30 pages. Airmail additional. Make checks payable to the American Institute of Physics.

[26] W. Gordy and R. L. Cook, *Microwave Molecular Spectra*, 3rd ed. (Wiley-Interscience, New York, 1984).

[27] R. F. Curl, Jr., J. Chem. Phys. **37**, 779 (1962).